

DREAM: Where Visual Understanding Meets Text-to-Image Generation

Chao Li^{1,*}, Tianhong Li¹, Sai Vidyaranya Nuthalapati², Hong-You Chen², Satya Narayan Shukla², Yonghuan Yang², Jun Xiao², Xiangjun Fan², Aashu Singh², Dina Katabi¹, Shlok Kumar Mishra²

¹MIT CSAIL, ²Meta AI

*Work done at Meta

Unifying visual representation learning and text-to-image (T2I) generation within a single model remains a central challenge in multimodal learning. We introduce **DREAM**, a unified framework that jointly optimizes discriminative and generative objectives, while learning strong visual representations. DREAM is built on two key techniques: During training, **Masking Warmup**, a progressive masking schedule, begins with minimal masking to establish the contrastive alignment necessary for representation learning, then gradually transitions to full masking for stable generative training. At inference, DREAM employs **Semantically Aligned Decoding** to align partially masked image candidates with the target text and select the best one for further decoding, improving text–image fidelity (+6.3%) without external rerankers. Trained solely on CC12M, DREAM achieves 72.7% ImageNet linear-probing accuracy (+1.1% over CLIP) and an FID of 4.25 (+6.2% over FLUID), with consistent gains in few-shot classification, semantic segmentation, and depth estimation. These results demonstrate that discriminative and generative objectives can be *synergistic*, allowing unified multimodal models that excel at both visual understanding and generation.

Date: March 4, 2026

Correspondence: Chao Li at chaoli@mit.edu

Code: <https://github.com/chaoli-charlie/dream>



1 Introduction

The evolution of multimodal learning has been marked by a recurring split between **models that represent** and **models that generate**. Discriminative vision–language systems such as CLIP (Radford et al. (2021)) utilize contrastive alignment to learn semantically rich representations, while text-to-image (T2I) generative models, including diffusion-based systems (Ramesh et al. (2022); Saharia et al. (2022)) and masked autoregressive (MAR) approaches (Fan et al. (2024)), produce high-fidelity images by learning conditional data distributions. Despite progress, unifying strong visual understanding and high-quality T2I generation within a single, fully trainable architecture remains an open challenge (Chen et al. (2023); Fan et al. (2024)).

This separation stems from an **optimization mismatch** between contrastive alignment, which necessitates minimal data corruption (Li et al. (2023a)), and generative modeling, which relies on aggressive masking (Li et al. (2024)) or noise injection (Ho et al. (2020)) to learn the underlying distribution. Consequently, naive optimization often leads to an unstable co-optimization where the model either achieves alignment but weak synthesis, or regresses toward generative-only representations. Recent efforts address this tension by freezing the vision encoder (Zheng et al. (2025)), but this design choice limits the potential for synergistic representations that could emerge from end-to-end joint optimization.

In this work, we demonstrate that this conflict can be effectively addressed through careful management of temporal optimization dynamics. We introduce **DREAM**, a unified framework that reconciles contrastive semantics with MAR-style generation through **Masking Warmup**. We begin training with low masking ratios ($\sim 15\%$) to prioritize learning robust contrastive features for image–text alignment. Over training, the masking ratio is sampled from a truncated Gaussian distribution whose mean increases linearly, allowing the model to gradually incorporate generative objectives. Once the distribution reaches the high-mask regime ($\sim 75\%$), it remains fixed, preventing interference with learned alignment features while enabling continued refinement of generative capacity. This progression ensures the model first establishes a semantic anchor before mastering dense reconstruction.

When trained on CC12M (Changpinyo et al. (2021)), our framework achieves **72.7% ImageNet-1K linear probing accuracy** (surpassing CLIP by 1.1%) and a **Text-to-Image FID of 4.25** (improving upon FLUID by 6.2%). Furthermore, as illustrated in Fig. 1, DREAM demonstrates consistent gains in few-shot classification, semantic segmentation, and depth estimation, suggesting that generative signals enhance the robustness of the underlying spatial representations

Beyond joint training, our unified architecture enables a novel inference-time strategy we term **Semantically Aligned Decoding**, which leverages DREAM’s internal contrastive representations to guide generation. Unlike prior work that relies on external CLIP-based reranking (Ramesh et al. (2022); Chang et al. (2022)), our method evaluates partially decoded candidates using the model’s own alignment knowledge, eliminating the need for auxiliary models. This self-guided approach improves text–image fidelity by **6.3%** while achieving **10.1% higher throughput** compared to methods requiring external guidance—demonstrating both effectiveness and efficiency gains from our unified design. We summarize our contributions as follows.

- **Unified Multimodal Framework through Masking Warmup:** We unify visual representation learning and T2I generation for masked autoregressive (MAR) models using a masking warmup schedule that effectively reconciles the tension between objectives while maintaining stability even when the mask remains fixed at its peak.
- **Semantically Aligned Decoding:** We introduce a zero-shot, self-guided decoding strategy that exploits the model’s internal contrastive representations for generation guidance, demonstrating superior computational efficiency and effectiveness compared to external CLIP rerankers.
- **Comprehensive Empirical Validation:** We extensively evaluate our unified framework against self-supervised and generative baselines demonstrating its superior performance on classical discriminative metrics (linear probing, fine-tuning, few-shot classification, semantic segmentation, and depth estimation) as well as on generation metrics (Fréchet Inception Distance (FID) and CLIP Score (CS)).

2 Related Work

Self-supervised Learning in Computer Vision. Self-supervised learning (SSL) has become a powerful paradigm for learning visual representations from unlabeled data by exploiting intrinsic image structure. Early contrastive methods such as SimCLR (Chen et al. (2020)) and MoCo (He et al. (2020)) maximize agreement between augmented views of the same image while repelling negatives. Later non-contrastive approaches such as BYOL (Grill et al. (2020)), SwAV (Caron et al. (2020)), and DINO (Caron et al. (2021)) remove explicit negatives, simplifying training while maintaining strong performance. CLIP (Radford et al. (2021)) marked a paradigm shift by applying contrastive learning to paired image–text data, yielding semantically rich representations that now underpin many vision–language and generative models.

Text-to-Image Generation. Modern T2I generation is largely driven by diffusion-based architectures (Rombach et al. (2022); Ramesh et al. (2022)), which achieve photorealistic results via iterative denoising but incur high sampling cost. Autoregressive (Fan et al. (2024)) and masked token prediction methods (Chang et al. (2022, 2023)) improve efficiency by generating image tokens in parallel or adaptive orders, narrowing the quality gap with diffusion. Recent work has shifted from discrete to continuous token representations to further boost quality: MAR (Li et al. (2024)) shows that continuous-token autoregressive modeling with high masking ratios yields state-of-the-art class-conditional generation, with FLUID (Fan et al. (2024)) demonstrating that this paradigm leads to more effective text-conditional generation than discrete tokenization approaches.

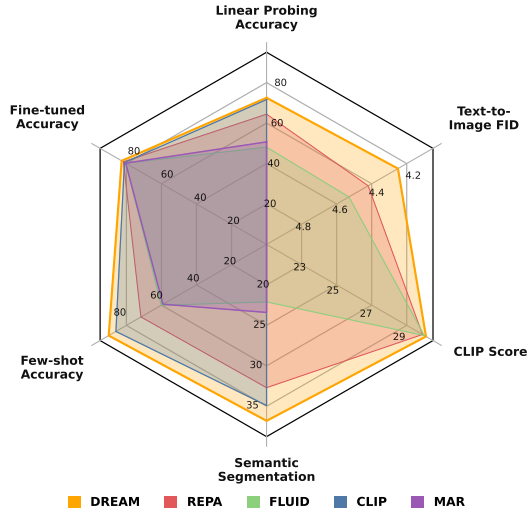


Figure 1 Performance of self-supervised and text-to-image generative models trained on CC12M. DREAM (yellow) forms the outer envelope across both discriminative and generative axes, outperforming all baselines and unifying strong visual understanding with high-quality text-to-image generation.

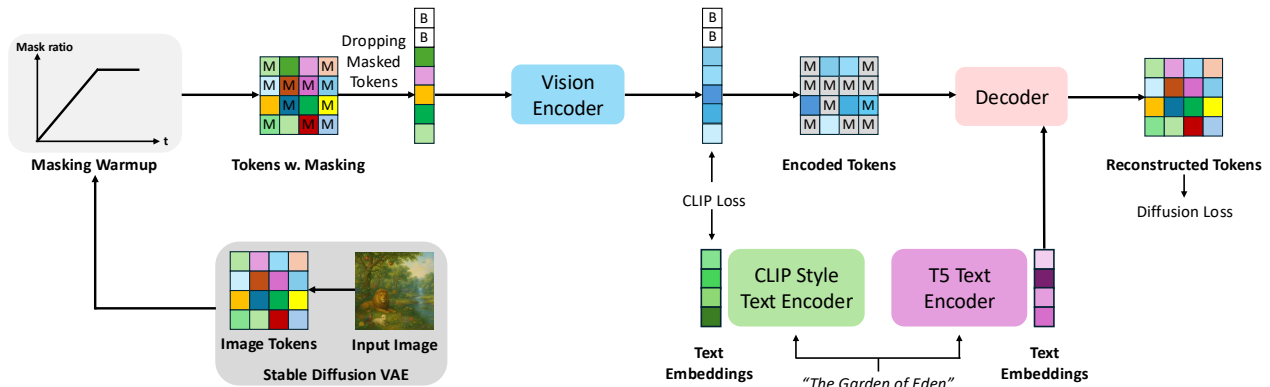


Figure 2 DREAM framework. Images are encoded into continuous tokens via Stable Diffusion VAE and randomly masked following a masking warmup schedule. The vision encoder is trained contrastively with text, and the decoder conditions on text to predict masked tokens with a diffusion-based reconstructive loss. Text conditioning is applied only in the decoder, ensuring the encoder learns visual representations without a text shortcut.

Unifying Representation and Generation. A growing line of work explores the synergy between self-supervised representation learning and generative modeling. Early efforts mostly focus on single-modality settings: MAGE (Li et al. (2023a)) extends masked image modeling to support both generation and recognition, while M3AE (Geng et al. (2022)) combines masked autoencoding with contrastive objectives in a unified vision–language framework, though its representations transfer less effectively than CLIP’s. More recent multimodal models such as Janus (Wu et al. (2025a)), Show-o (Xie et al. (2024)), and Harmon (Wu et al. (2025b)) aim to unify discriminative understanding and T2I generation. These works are important steps forward but mainly target VQA-style tasks (answering questions about an image) rather than core visual discriminative tasks such as classification, segmentation, and depth estimation. Recent studies show that strong VQA performance can often be achieved by leveraging text priors in the text encoder, even when the vision encoder underperforms on classification or depth estimation (Fu et al. (2025); Zhang et al. (2024)). REPA (Yu et al. (2025)) couples representation quality and generation fidelity by injecting DINO-v2 features into diffusion transformer latents, improving stability and sample quality, while RAE (Zheng et al. (2025)) uses frozen DINO-v2 encoders for T2I generation. We compare DREAM directly with REPA, and indirectly with Harmon and Janus, which use frozen vision encoders from MAR and CLIP, respectively.

3 Method

DREAM adopts a ViT-based encoder–decoder architecture over continuous image latents. The encoder learns language-aligned visual features, and the decoder generates images conditioned on text through a diffusion based reconstruction loss. Importantly, text conditioning is applied only in the decoder, ensuring the encoder learns visual representations without relying on language shortcuts (see Fig. 2).

3.1 Architecture

Continuous Tokenization. We encode images into continuous latent representations using the pretrained VAE encoder from Stable Diffusion (Rombach et al. (2022)). This continuous tokenization preserves fine-grained spatial information while maintaining computational efficiency.

Vision Encoder. Our encoder follows MAR’s architecture (Li et al. (2023a)). We prepend learnable buffer tokens [B] to the encoder input to enhance representation capacity and training stability. The encoder processes only the buffer tokens and the unmasked tokens.

Text Encoders. We employ two text encoders with distinct roles in training. For **contrastive alignment**, captions are tokenized using the OpenAI CLIP tokenizer (Radford et al. (2021)) (77 tokens) and encoded by a CLIP text transformer following (Tian et al. (2023)), projecting the text features into the vision encoder’s latent space. For **generation**, captions are tokenized with SentencePiece (Kudo and Richardson (2018)) (128 tokens) and encoded by a frozen T5-XXL (Raffel

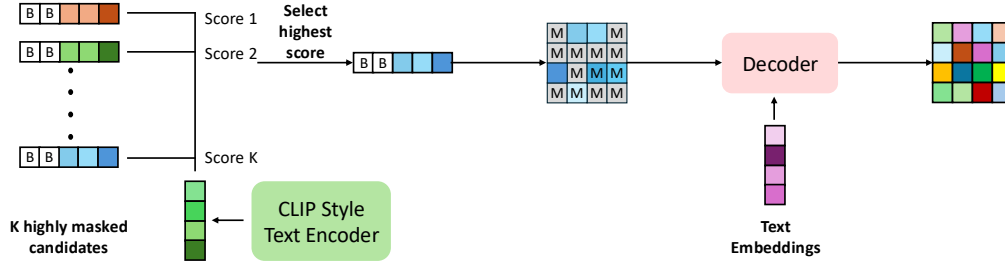


Figure 3 Semantically Aligned Decoding. The model spawns K parallel candidates, each partially decoded to an intermediate timestep t . The encoder scores each candidate by comparing its visual embedding to the prompt embedding, and the top-scoring candidate is fully decoded—improving image fidelity and text alignment without external rerankers.

et al. (2020)). A lightweight 6-layer text aligner then projects the T5 embeddings into the decoder’s latent space, providing conditioning for masked autoregressive generation.

Text-to-Image Decoder. Our decoder adopts FLUID’s architecture but is paired with the encoder described above, forming a unified encoder–decoder model. Each block comprises self-attention, cross-attention, and feed-forward layers. Self-attention operates on visual tokens, while cross-attention conditions generation on text features. During training, masked visual tokens are replaced with a learnable token, and the decoder predicts these masked tokens using bidirectional attention, similar to BERT. The encoder and decoder each contain half of the total transformer blocks. Our Large (L) configuration uses 32 layers (16 per module) with a hidden width of 1024, totaling 570M parameters.

Output Head. To predict continuous latent tokens, we attach a lightweight six-layer MLP diffusion head (Li et al. (2024)) that matches the transformer’s embedding dimension. The diffusion process follows the improved DDPM formulation (Nichol and Dhariwal (2021); Li et al. (2024)), using a cosine noise schedule with 1000 steps during training and 100 resampled steps during inference.

3.2 Training Objectives

Diffusion Reconstruction Loss We adopt the same diffusion loss used in (Li et al. (2024); Fan et al. (2024)), where the conditional distribution $p(x | z)$ via denoising is modelled as follows:

$$\mathcal{L}_{\text{diff}}(z, x) = \mathbb{E}_{\epsilon, t} [\|\epsilon - \epsilon_{\theta}(x_t | t, z)\|^2] \quad (1)$$

where $\epsilon \sim \mathcal{N}(0, I)$ is Gaussian noise, and $x_t = \sqrt{\bar{\alpha}_t}x + \sqrt{1 - \bar{\alpha}_t}\epsilon$ represents the noisy latent at timestep t under variance schedule $\bar{\alpha}_t$. The denoising network ϵ_{θ} predicts noise conditioned on encoder embeddings z , enabling end-to-end gradient. We sample four independent noise levels per image to improve gradient estimates without recomputing z .

We compute diffusion loss for samples that has greater than 50% of its tokens masked, since high masking ratios are essential for effective generative modeling (Li et al. (2024)).

Contrastive Learning We further incorporate CLIP-style contrastive learning (Radford et al. (2021)) to align image and text representations. Given N paired samples (x_i^I, x_i^T) , we compute the InfoNCE loss as:

$$\mathcal{L}_I = - \sum_{i=1}^N \log \frac{e^{\text{sim}(f_I(\text{aug}_I(x_i^I)), f_T(x_i^T)) / \tau}}{\sum_{k=1}^N e^{\text{sim}(f_I(\text{aug}_I(x_i^I)), f_T(x_k^T)) / \tau}} \quad (2)$$

where $\text{sim}(\cdot, \cdot)$ denotes cosine similarity and τ is a learnable temperature parameter. A symmetric text-to-image term \mathcal{L}_T is computed analogously, and the final contrastive objective is $\mathcal{L}_{\text{clip}} = (\mathcal{L}_I + \mathcal{L}_T) / 2$.

We cap the maximum masking ratio at 75% for CLIP loss computation, as excessive masking degrades discriminative learning (Li et al. (2023b,a)).

Table 1 Quantitative comparison of self-supervised and text-to-image models trained on CC12M. We evaluate models on two tasks: visual understanding, measured by linear probing (“LP”) and fine-tuned (“FT”) accuracy on ImageNet-1K, and image generation, evaluated using FID and CLIP Score (CS) on CC12M and zero-shot MS-COCO. Metrics shown in blue are computed over 40K samples. DREAM achieves strong performance on both tasks, outperforming specialized generative models while maintaining competitive representation quality, including against methods that use additional supervision[†]. “X” indicates models without text-to-image capability, and “-” denotes unreported results.

	Model	Visual Understanding		Text-to-Image Generation			
		IN-1K		CC12M-50K		MS-COCO-30K	
		LP [↑]	FT [↑]	FID [↓]	CS [↑]	FID [↓]	CS [↑]
Generation only	LPL Berrada et al. (2025)	-	-	6.22	25.1	-	-
	SDXL Ifriqi et al. (2024)	-	-	8.53	-	-	25.4
	mmDiT-SD3 Ifriqi et al. (2024)	-	-	7.54	-	-	24.8
	mmDiT-Imp Ifriqi et al. (2024)	-	-	6.79	-	-	26.6
	GALIP Tao et al. (2023)	-	-	-	-	14.6	29.3
	SCAD Kobayashi et al. (2025)	-	-	-	-	12.3	27.6
Representation only	MAE-L/16 Tian et al. (2023)	50.7	76.8	X	X	X	X
	M3AE-L/16 Geng et al. (2022)	64.1	77.1	X	X	X	X
	SimCLR-L/16 Tian et al. (2023)	61.5	-	X	X	X	X
	StableRep-L/16 [†] Tian et al. (2023)	74.7	-	X	X	X	X
	LaCLIP-L/16 [†] Fan et al. (2023)	73.7	-	X	X	X	X
Unified	4M-L [†] Mizrahi et al. (2023)	-	86.6	11.9*	18.9	30.1	23.1
	DREAM	72.7	82.7	4.25 (5.16*)	30.1	10.4	31.5

[†] Trained with extra labels.

* FID computed over 30K samples

Joint Optimization The total loss jointly optimizes generation and alignment:

$$\mathcal{L} = \mathcal{L}_{\text{diff}} + \lambda \cdot \mathcal{L}_{\text{clip}}, \quad (3)$$

where λ balances the diffusion and contrastive terms.

3.3 Masking Warmup

A key challenge in joint training is the conflicting requirements of two objectives: contrastive learning benefits from complete visual context, while generative modeling requires aggressive masking. We address this through a masking warmup schedule that gradually increases to a fixed stable value for the rest of training. The masking ratio is sampled from a truncated Gaussian distribution ($\sigma = 0.55$, range $[0, 1.0]$). The mean of the distribution increases linearly from 0 to 1.0 over the first 36 epochs. After that point, the mean is fixed at 1.0, corresponding to fully masked images.

3.4 Inference

Representation Extraction. For linear probing and finetuning, encoder output features are globally average-pooled and fed into task-specific heads (linear probes or fine-tuned classifiers). For semantic segmentation and depth estimation, we freeze the vision encoder and evaluate features and follow the linear-probe protocol of (Siméoni et al. (2025)).

Image Generation. For image generation, DREAM follows MAR’s next set-of-tokens prediction strategy (Li et al. (2024)): starting from a fully masked sequence, the masking ratio is annealed from 1.0 to 0 using a cosine schedule (Chang et al. (2022); Li et al. (2023a)) over 64 steps by default. Decoding uses temperature sampling and fully randomized token orders at every step, as in MAR.

Semantically Aligned Decoding. We introduce a zero-shot semantically decoding strategy that selects the most text-aligned candidate during the decoding process. As illustrated in Fig. 3, given a prompt, DREAM spawns K candidates— independent decoding trajectories initialized by different stochastic seeds. After a small fraction of the 64 decoding steps ($t \ll 64$), DREAM produces partially decoded latents for all K candidates. These partial latents are fed

Table 2 Unified evaluation of Visual Understanding and Text-to-Image generation. Comparison of models trained on CC12M across two paradigms: (a) *Visual Understanding*, measured by Top-1 accuracy (%) on ImageNet and its robustness benchmarks; and (b) *Text-to-Image Generation*, measured by FID and CLIP Score (CS) on CC12M and zero-shot MS-COCO. FID and CS for CC12M were computed over 50K samples, and FID and CS for MS-COCO were computed over 30K samples. **X** indicates models inherently incapable of Text-to-Image generation.

Model	Visual Understanding											Text-to-Image Generation			
	LP \uparrow		FT \uparrow									CC12M		MS-COCO	
	IN-1K	IN-1K	IN-A	IN-R	IN-S	IN-H	MF	T7	Top	ON	Avg.	FID \downarrow	CS \uparrow	FID \downarrow	CS \uparrow
MAR	50.7	80.4	20.6	44.6	29.4	21.1	69.0	77.0	81.7	37.4	51.2	X	X	X	X
FLUID	48.1	80.3	20.2	44.2	28.6	21.1	68.9	77.3	81.6	37.6	51.1	4.53	30.0	9.62	30.7
CLIP	71.6	81.1	24.3	53.9	40.8	23.3	69.3	77.1	81.7	37.8	54.4	X	X	X	X
REPA	62.5 [†]	81.7	27.7	51.2	37.2	23.1	71.0	79.1	83.1	39.1	54.8	4.42	29.9	10.0	30.7
DREAM	72.7	82.7	32.8	55.3	42.0	26.0	71.7	79.4	83.5	41.3	57.2	4.25	30.1	10.4	31.5

Benchmarks: IN-1K [Deng et al. \(2009b\)](#), IN-A [Hendrycks et al. \(2021b\)](#), IN-R [Hendrycks et al. \(2021a\)](#), IN-S [Wang et al. \(2019a\)](#), IN-H [Taesiri et al. \(2023\)](#), MF/T7/Top [Recht et al. \(2019\)](#), and ON [Barbu et al. \(2019\)](#).

[†] REPA’s linear probe was additionally evaluated on the CLIP-aligned encoder layer, yielding a slightly higher accuracy of 64.4.

to the vision encoder to obtain visual representations, which are scored for text–image alignment against the prompt using DREAM’s contrastive text encoder (shown to reliably retrieve partially decoded images; (see Fig. 7). Only the top-scoring candidate continue for the remaining decoding steps to reach the full image.

This approach fundamentally differs from prior candidate ranking methods ([Chang et al. \(2023\)](#); [Ramesh et al. \(2022\)](#)) in two ways: (1) selection occurs at the latent level with a fraction of the image decoded, avoiding the cost of generating complete images; (2) the model uses its own learned alignment rather than external vision-language models.

4 Experiments and Results

4.1 Implementation Details

Data. We train on Conceptual 12M (CC12M) ([Changpinyo et al. \(2021\)](#)), containing 11.3M image-text pairs. Images are center-cropped to 256×256 with horizontal flipping as augmentation ([Li et al. \(2024\)](#)). We evaluate representations on ImageNet-1K ([Deng et al. \(2009a\)](#)) and generation quality on CC12M and MS-COCO ([Lin et al. \(2014\)](#)).

Training. All models are trained for 49 epochs using AdamW optimizer ($\beta_1 = 0.9, \beta_2 = 0.95$) ([Loshchilov and Hutter \(2017\)](#)) with batch size 2048. We employ a constant learning rate with 12-epoch linear warmup to a maximum of 8×10^{-4} . DREAM additionally employs the 36-epoch progressive masking warmup described above. Evaluation uses the exponential moving average (EMA) of model weights with a decay rate of 0.9999.

4.2 Unified Performance

Table 1 presents a comprehensive comparison of DREAM against existing models trained on CC12M, covering both discriminative and generative benchmarks. As shown, most prior T2I models trained on CC12M focus solely on generation quality and rarely evaluate the discriminative strength of their vision encoders. In contrast, DREAM achieves superior linear probing and fine-tuned classification accuracy compared to other representation-learning models, without relying on additional labels or supervision. On the generative side, DREAM outperforms both generative-only models such as LPL (FID: +31.7%, CS: +19.9% on CC12M) and SCAD (FID: +15.7%, CS: +14.1% on MS-COCO).

4.3 Discriminative Representations

Below, we analyze DREAM’s learned representations and generative behavior across three baseline families: (1) contrastive-only (CLIP), (2) generative-only (MAR, FLUID), and (3) representation-aligned generative (REPA).

All baselines share the same encoder–decoder Transformer architecture and differ only in objective and conditioning. CLIP uses the encoder with a contrastive loss, yielding strong representations but no generation. MAR, originally

class-conditioned, is reimplemented without class conditioning. FLUID, decoder-only, is adapted to an encoder–decoder setup; it can be viewed as MAR with text conditioning added to the decoder, ensuring the encoder learns representations without a text shortcut. DREAM builds on FLUID by introducing Masking Warmup and applying the CLIP contrastive loss to the encoder’s final layer.

REPA extends FLUID by aligning intermediate encoder features, specifically the unmasked tokens at layer 6, with those from a pretrained CLIP-L encoder (Radford et al. (2021)). Originally developed for class-conditioned diffusion (Yu et al. (2025)), it is adapted here with text conditioning. We employ CLIP-L as the teacher model, rather than the default DINO-v2 teacher used in (Yu et al. (2025)), as it empirically yields stronger text-to-image generation fidelity in our setting (Refer to Section A.2.3).

Since CLIP and MAR lack T2I capability, we evaluate only their encoder representations, while FLUID, REPA, and DREAM are assessed on both discriminative and generative benchmarks.

Linear Probing. Linear probing is a standard evaluation protocol for assessing the intrinsic quality of visual representations learned in a self-supervised manner. As shown in Table 2, generative models—both unconditional (MAR) and text-conditioned (FLUID)—fail to learn representations as strong as those from contrastive models like CLIP. In contrast, models trained with CLIP-style alignment objectives (REPA and DREAM) achieve substantially higher linear probing accuracy as compared to their generative baselines. We also observe that SD-VAE tokenization did not hurt CLIP performance given that we were able to reproduce the Linear Probing accuracy of CLIP trained on pixels in StableRep (Tian et al. (2023)) with SD-VAE tokens.

DREAM attains 72.7% linear probing accuracy, surpassing its generative baseline FLUID by 28.6%. Moreover, DREAM exceeds CLIP by 1.1%, despite sharing the same contrastive objective. This highlights that coupling language-aligned contrastive learning with diffusion-based reconstruction yields more semantically coherent and transferable visual representations.

Fine-tuning. Following the protocol of (Li et al. (2023a)), we fine-tune all models on ImageNet-1K and evaluate their robustness on multiple out-of-domain ImageNet variants. As shown in Table 2, DREAM not only achieves strong in-domain performance—surpassing CLIP by +1.6% and REPA by +1.0% on ImageNet-1K—but also demonstrates markedly superior generalization to distribution shifts.

Across all out-of-domain benchmarks, DREAM consistently delivers the highest accuracy, outperforming CLIP by +2.8% and REPA by +2.4% on average. Models trained with CLIP-style alignment (REPA and DREAM) reliably exceed both CLIP and their generative-only counterparts after finetuning, confirming that integrating a generative objective is synergetic with learning robust, transferable visual features. DREAM’s gains are especially pronounced on the most challenging variants (IN-A and IN-H), underscoring its ability to generalize beyond the training distribution.

Few-shot Learning. Prior work has established that high-quality representations are critical for few-shot image classification (Wang et al. (2019b); Tian et al. (2020); Dhillon et al. (2019)). A simple linear classifier trained on frozen features can achieve competitive performance. Following the standard 5-way, 5-shot protocol (Tian et al. (2023); Wang et al. (2019b); El Banani et al. (2023)), we evaluate DREAM across 14 benchmark datasets. As shown in Table 3, DREAM consistently outperforms all baselines across all datasets. Notably, it outperforms the next best model CLIP by a significant margin (+4.1%).

Dense Prediction Table 9 reports results on dense prediction tasks. DREAM achieves 36.8% mIoU on ADE20K (+1.9 over CLIP) and an RMSE of 0.60 on NYU Depth v2, matching REPA while outperforming CLIP by 6.25%. These gains indicate that the diffusion reconstruction objective enhances spatial grounding, as denoising full images encourages the encoder to learn pixel-aligned features that transfer effectively to dense prediction.

Zero-shot Robustness. Since DREAM is trained with variable masking ratios, it is more resilient under heavy occlusion. We compare standard CLIP, CLIP with masking warm-up (CLIP-M), and DREAM by evaluating zero-shot accuracy across masking levels (Fig. 7). Progressive warm-up improves robustness for both CLIP-M and DREAM over CLIP, with gains of roughly 0.7% once more than 20% of the image is masked. DREAM consistently outperforms CLIP-M across all masking levels, reflecting the benefit of locally grounded representations learned via diffusion-based reconstruction. This advantage becomes pronounced at extreme occlusion (masking ratio > 0.8), where DREAM achieves over 6.2× the zero-shot accuracy of CLIP, highlighting the resilience conferred by joint contrastive–generative training.

Table 3 Few-shot transfer evaluation of different models. We report 5-way, 5-shot classification accuracy across 14 datasets. We highlight the best performance of each dataset in bold. DREAM outperforms the other models in most of the datasets.

Model	DTD	Caltech-256	SUN397	Food-101	VOC2007	STL-10	Flowers	UC Merced	EuroSAT	Country211	RESISC45	Dogs	MIT Indoors	IN-1K	Average
MAR	64.9	56.1	73.0	42.3	47.2	53.1	74.6	77.3	74.9	28.9	73.8	37.7	61.2	62.3	59.1
FLUID	66.3	58.0	73.7	43.7	47.9	53.7	76.1	77.0	75.8	29.4	74.4	38.9	62.7	64.1	60.1
CLIP	81.0	95.1	95.8	86.0	79.6	96.1	96.2	92.6	82.1	42.9	90.4	78.2	93.7	94.3	86.0
REPA	73.2	73.6	88.1	60.2	61.2	74.6	86.5	82.4	79.2	33.8	80.4	50.2	81.2	78.9	71.7
DREAM	88.6	96.4	97.3	86.9	95.0	99.8	95.9	98.5	95.0	42.9	93.4	81.2	94.5	96.1	90.1

4.4 T2I Generation

We evaluate DREAM’s text-to-image generation on CC12M and MS-COCO using FID and CLIP Score (CS) following (Chang et al. (2023)). As shown in Table 2, DREAM achieves the best results on CC12M, with an FID of 4.25 and CS of 30.1, outperforming generative baselines FLUID and REPA. Compared to FLUID, DREAM improves FID by 0.28 (+6.2%) with a slight gain in CS, indicating that coupling contrastive alignment with generative training enhances reconstruction fidelity without harming semantic alignment. REPA attains an FID of 4.42, consistent with prior reports (Yu et al. (2025)), but remains weaker than DREAM (-4%).

On MS-COCO zero-shot generation, DREAM achieves the highest CS (31.5) and competitive FID (10.4), within 0.8 of FLUID. Interestingly, REPA—also a representation alignment method—shows a similar trend: strong FID on CC12M but weaker performance on MS-COCO, suggesting that representation-driven priors can be sensitive to domain and caption mismatch between CC12M and COCO. In contrast, DREAM maintains stronger text-image alignment under this shift than REPA, as reflected in its higher CS.

5 Analysis

We analyze DREAM’s design choices to clarify the principles enabling unified representation-generation learning. We examine: (1) whether gains from joint optimization scale with model size; (2) how the masking schedule and loss hyperparameters influence the representation-generation trade-off; and (3) how semantic guidance during decoding affects generation quality under a fixed compute budget.

Unless otherwise noted, ablations use DREAM-L trained for 49 epochs on CC12M with the standard configuration: masking standard deviation $\sigma = 0.45$, CLIP loss weight $\lambda = 0.005$, and generation without Semantically Aligned Decoding. This differs from the main setup in Section 4, which uses $\sigma = 0.55$ with Semantically Aligned Decoding; absolute values shift, but relative trends remain consistent. Additional ablations are provided in the Appendix.

5.1 Scaling Behavior

Fig. 4 shows that DREAM scales effectively for both representation and generation. Linear probing accuracy increases monotonically with model size, following standard scaling trends. Generation quality likewise improves: FID drops from 5.67 (DREAM-B) to 4.89 (DREAM-G), matching purely generative baselines such as FLUID. These results indicate that contrastive and generative objectives are synergistic rather than competing for capacity.

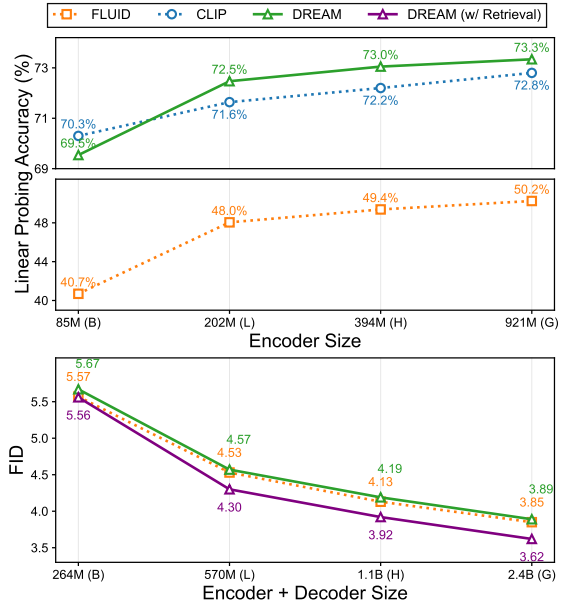


Figure 4 Performance of DREAM across different model sizes (B/L/H/G) for $\sigma=0.45$. Top: Linear Probing on IN-1K. Bottom: FID on CC12M-50K with and without Semantically Aligned Decoding. DREAM consistently outperforms baselines on both metrics across different sizes.

Semantically Aligned Decoding provides consistent gains across all scales, enabling DREAM to surpass FLUID by substantial margins (+6.2% on **L**, +5.0% on **H**, and +6.0% on **G**). This suggests that semantic guidance fundamentally enhances generation, rather than being an artifact of a particular model size.

5.2 Key Design Ablations

5.2.1 Masking Schedule Design.

Unifying representation learning and T2I generation is challenging because the two objectives favor opposite masking regimes. To study this trade-off, we compare four masking strategies on DREAM: **FX**, a fixed truncated Gaussian as in FLUID; **UNI**, a uniform distribution; **CD**, a cooldown schedule that decreases masking over time; and our proposed **WM**, which progressively increases the masking ratio.

Table 4 Effect of Masking Schedule

	FX	UNI	CD	WM
LP \uparrow	4.6	73.1	73.1	72.5
FID \downarrow	N/A	4.88	5.80	4.57

As shown in Table 4, **FX** masking which naively combines high masking with a contrastive loss leads to unstable training and poor performance in both representation learning and generation. In contrast, **UNI** and **CD** train stably but underperform the FLUID baseline in generative quality (FID = 4.53; Table 2), as they insufficiently emphasize sustained high-masking regimes (FID -6.8% and -18.9% vs. **WM**). Evidently, **WM** resolves this conflict improving on both the representation and generation front while retaining stable joint optimization throughout the course of training (Refer to Fig. 6)

5.2.2 Effect of Diffusion Reconstruction

We further show that DREAM’s gains in representation learning do not stem from masking warmup alone, but from the synergistic co-optimization of contrastive learning and generative reconstruction. To isolate this effect, we compare three models: (1) a CLIP baseline, (2) CLIP-M, which applies masking warmup to CLIP, and (3) DREAM, which incorporates warmup by design.

Table 5 Effect of Masking Warmup and Diffusion Loss

	CLIP	CLIP-M	DREAM
LP \uparrow	71.6	70.8	72.5
FID \downarrow	N/A	N/A	4.57

As shown in Table 5, naively adding masking warmup to CLIP degrades performance, as the high masking regime later in training disrupts discriminative representations. In contrast, DREAM leverages high masking to learn robust representations, enabled by the diffusion reconstruction loss, which stabilizes training and provides complementary generative supervision.

5.2.3 Efficiency of Semantically Aligned Decoding

Finally, we compare DREAM decoding with an external CLIP reranker under a fixed compute budget measured by the number of forward encoder (NFE) passes. As shown in Table 6, DREAM achieves higher throughput than CLIP reranking under the same NFE budget, both with and without Semantically Aligned Decoding (SD).

This efficiency gain arises because external CLIP reranking can only score fully generated images, requiring all candidates to be decoded before selection. In contrast, DREAM evaluates candidates directly in the latent space using partially generated image embeddings, avoiding redundant full generations and reducing decoding overhead. Consequently, DREAM maintains higher throughput even for $K = 1$, with additional benefits as K increases. Moreover, under a fixed budget, increasing K has minimal impact on throughput (1.77–1.86 images/sec), indicating good scalability.

Table 6 Efficiency of DREAM decoding under fixed compute budgets (A100 GPU). We compare the throughput (images/sec), FID, and CLIP Score (CS) for varying candidate counts K against using pretrained CLIP as external reranker. **SD**: Semantically Aligned Decoding.

Method	Throughput	FID ↓	CLIP ↑
<i>64 NFE Passes</i>			
DREAM (K=1)	3.39	4.57	29.1
<i>128 NFE Passes</i>			
DREAM (K=1)	1.77	4.34	29.4
DREAM (K=2 w./ Ext. CLIP) [†]	1.69	4.50	29.6
DREAM (K=9 w./ SD)	1.86	4.25	30.1
DREAM (K=17 w./ SD)	1.85	4.37	30.3

[†] Uses an external model to select image candidates.

In terms of quality, DREAM without SD ($K = 1$) already outperforms CLIP reranking under the same 128 NFE budget in FID (4.34 vs. 4.50). With SD enabled, DREAM ($K = 9$) further improves both fidelity and semantic alignment, achieving a 5.6% reduction in FID and a 1.7% increase in CLIP score while maintaining comparable throughput. Overall, DREAM provides a more efficient and effective alternative to post-hoc CLIP-based reranking.

6 Conclusion

We introduced DREAM, a unified multimodal framework for representation learning and text-to-image generation. By reconciling contrastive and generative objectives through Masking Warmup and improving inference via Semantically Aligned Decoding, DREAM shows that strong discriminative understanding and high-fidelity generation can coexist within a single architecture. We hope DREAM serves as a step toward more general-purpose vision–language systems and can be extended by scaling to larger paired datasets.

References

- Hangbo Bao, Li Dong, Songhao Piao, and Furu Wei. Beit: Bert pre-training of image transformers. *arXiv preprint arXiv:2106.08254*, 2021.
- Andrei Barbu, David Mayo, Julian Alverio, William Luo, Christopher Wang, Dan Gutfreund, Josh Tenenbaum, and Boris Katz. Objectnet: A large-scale bias-controlled dataset for pushing the limits of object recognition models. *Advances in neural information processing systems*, 32, 2019.
- Tariq Berrada, Pietro Astolfi, Melissa Hall, Marton Havasi, Yohann Benchetrit, Adriana Romero-Soriano, Karteek Alahari, Michal Drozdal, and Jakob Verbeek. Boosting latent diffusion with perceptual objectives. In *The Thirteenth International Conference on Learning Representations*, 2025.
- Mathilde Caron, Ishan Misra, Julien Mairal, Priya Goyal, Piotr Bojanowski, and Armand Joulin. Unsupervised learning of visual features by contrasting cluster assignments. In *Advances in Neural Information Processing Systems (NeurIPS)*, 2020. https://papers.neurips.cc/paper_files/paper/2020/file/70feb62b69f16e0238f741fab228fec2-Paper.pdf.
- Mathilde Caron, Hugo Touvron, Ishan Misra, Hervé Jégou, Julien Mairal, Piotr Bojanowski, and Armand Joulin. Emerging properties in self-supervised vision transformers. In *Proceedings of the IEEE/CVF international conference on computer vision*, pages 9650–9660, 2021.
- Huiwen Chang, Han Zhang, Lu Jiang, Ce Liu, and William T Freeman. Maskgit: Masked generative image transformer. In *Proceedings of the IEEE/CVF conference on computer vision and pattern recognition*, pages 11315–11325, 2022.
- Huiwen Chang, Han Zhang, Jarred Barber, AJ Maschinot, Jose Lezama, Lu Jiang, Ming-Hsuan Yang, Kevin Murphy, William T Freeman, Michael Rubinstein, et al. Muse: Text-to-image generation via masked generative transformers. *arXiv preprint arXiv:2301.00704*, 2023.
- Soravit Changpinyo, Piyush Sharma, Nan Ding, and Radu Soricut. Conceptual 12M: Pushing web-scale image-text pre-training to recognize long-tail visual concepts. In *CVPR*, 2021.
- Fei-Long Chen, Du-Zhen Zhang, Ming-Lun Han, Xiu-Yi Chen, Jing Shi, Shuang Xu, and Bo Xu. Vlp: A survey on vision-language pre-training. *Machine Intelligence Research*, 20(1):38–56, 2023.
- Ting Chen, Simon Kornblith, Mohammad Norouzi, and Geoffrey Hinton. A simple framework for contrastive learning of visual representations. In *Proceedings of the 37th International Conference on Machine Learning (ICML)*, volume 119 of *PMLR*, pages 1597–1607, 2020. <https://proceedings.mlr.press/v119/chen20j/chen20j.pdf>.
- Ekin D Cubuk, Barret Zoph, Jonathon Shlens, and Quoc V Le. Randaugment: Practical automated data augmentation with a reduced search space. In *Proceedings of the IEEE/CVF conference on computer vision and pattern recognition workshops*, pages 702–703, 2020.
- Jia Deng, Wei Dong, Richard Socher, Li-Jia Li, Kai Li, and Li Fei-Fei. Imagenet: A large-scale hierarchical image database. In *2009 IEEE Conference on Computer Vision and Pattern Recognition*, pages 248–255, 2009a. doi: 10.1109/CVPR.2009.5206848.
- Jia Deng, Wei Dong, Richard Socher, Li-Jia Li, Kai Li, and Li Fei-Fei. Imagenet: A large-scale hierarchical image database. In *2009 IEEE conference on computer vision and pattern recognition*, pages 248–255. Ieee, 2009b.
- Guneet S Dhillon, Pratik Chaudhari, Avinash Ravichandran, and Stefano Soatto. A baseline for few-shot image classification. *arXiv preprint arXiv:1909.02729*, 2019.
- Alexey Dosovitskiy. An image is worth 16x16 words: Transformers for image recognition at scale. *arXiv preprint arXiv:2010.11929*, 2020.
- Mohamed El Banani, Karan Desai, and Justin Johnson. Learning visual representations via language-guided sampling. In *Proceedings of the IEEE/CVF conference on computer vision and pattern recognition*, pages 19208–19220, 2023.
- Lijie Fan, Dilip Krishnan, Phillip Isola, Dina Katabi, and Yonglong Tian. Improving clip training with language rewrites. *Advances in Neural Information Processing Systems*, 36:35544–35575, 2023.
- Lijie Fan, Tianhong Li, Siyang Qin, Yuanzhen Li, Chen Sun, Michael Rubinstein, Deqing Sun, Kaiming He, and Yonglong Tian. Fluid: Scaling autoregressive text-to-image generative models with continuous tokens. *arXiv preprint arXiv:2410.13863*, 2024.
- Stephanie Fu, Tyler Bonnen, Devin Guillory, and Trevor Darrell. Hidden in plain sight: Vlms overlook their visual representations, 2025. <https://arxiv.org/abs/2506.08008>.
- Xinyang Geng, Hao Liu, Lisa Lee, Dale Schuurmans, Sergey Levine, and Pieter Abbeel. Multimodal masked autoencoders learn transferable representations. *arXiv preprint arXiv:2205.14204*, 2022.

- Jean-Bastien Grill, Florian Strub, Florent Alché, Corentin Tallec, Pierre H. Richemond, Elena Buchatskaya, Carl Doersch, Bernardo Avila Pires, Zhaohan Daniel Guo, Mohammad Gheshlaghi Azar, Bilal Piot, Koray Kavukcuoglu, Rémi Munos, and Michal Valko. Bootstrap your own latent: A new approach to self-supervised learning. In *Advances in Neural Information Processing Systems (NeurIPS)*, 2020. <https://papers.nips.cc/paper/2020/file/f3ada80d5c4ee70142b17b8192b2958e-Paper.pdf>.
- Kaiming He, Haoqi Fan, Yuxin Wu, Saining Xie, and Ross Girshick. Momentum contrast for unsupervised visual representation learning. In *Proceedings of the IEEE/CVF Conference on Computer Vision and Pattern Recognition (CVPR)*, pages 9729–9738, 2020. https://openaccess.thecvf.com/content_CVPR_2020/papers/He_Momentum_Contrast_for_Unsupervised_Visual_Representation_Learning_CVPR_2020_paper.pdf.
- Dan Hendrycks, Steven Basart, Norman Mu, Saurav Kadavath, Frank Wang, Evan Dorundo, Rahul Desai, Tyler Zhu, Samyak Parajuli, Mike Guo, Dawn Song, Jacob Steinhardt, and Justin Gilmer. The many faces of robustness: A critical analysis of out-of-distribution generalization. *ICCV*, 2021a.
- Dan Hendrycks, Kevin Zhao, Steven Basart, Jacob Steinhardt, and Dawn Song. Natural adversarial examples. *CVPR*, 2021b.
- Jonathan Ho, Ajay Jain, and Pieter Abbeel. Denoising diffusion probabilistic models. In *NeurIPS*, 2020. <https://arxiv.org/abs/2006.11239>.
- Gao Huang, Yu Sun, Zhuang Liu, Daniel Sedra, and Kilian Q Weinberger. Deep networks with stochastic depth. In *European conference on computer vision*, pages 646–661. Springer, 2016.
- Tariq Berrada Ifriqi, Pietro Astolfi, Melissa Hall, Reyhane Askari-Hemmat, Yohann Benchetrit, Marton Havasi, Matthew Muckley, Karteek Alahari, Adriana Romero-Soriano, Jakob Verbeek, et al. On improved conditioning mechanisms and pre-training strategies for diffusion models. *arXiv preprint arXiv:2411.03177*, 2024.
- Yuya Kobayashi, Yuhta Takida, Takashi Shibuya, and Yuki Mitsufuji. Efficiency without compromise: Clip-aided text-to-image gans with increased diversity. *arXiv preprint arXiv:2506.01493*, 2025.
- Taku Kudo and John Richardson. Sentencepiece: A simple and language independent subword tokenizer and detokenizer for neural text processing. *arXiv preprint arXiv:1808.06226*, 2018.
- Tianhong Li, Huiwen Chang, Shlok Mishra, Han Zhang, Dina Katabi, and Dilip Krishnan. Mage: Masked generative encoder to unify representation learning and image synthesis. In *Proceedings of the IEEE/CVF Conference on Computer Vision and Pattern Recognition*, pages 2142–2152, 2023a.
- Tianhong Li, Yonglong Tian, He Li, Mingyang Deng, and Kaiming He. Autoregressive image generation without vector quantization. *Advances in Neural Information Processing Systems*, 37:56424–56445, 2024.
- Yanghao Li, Haoqi Fan, Ronghang Hu, Christoph Feichtenhofer, and Kaiming He. Scaling language-image pre-training via masking. In *Proceedings of the IEEE/CVF conference on computer vision and pattern recognition*, pages 23390–23400, 2023b.
- Tsung-Yi Lin, Michael Maire, Serge Belongie, James Hays, Pietro Perona, Deva Ramanan, Piotr Dollár, and C Lawrence Zitnick. Microsoft coco: Common objects in context. In *European conference on computer vision*, pages 740–755. Springer, 2014.
- Ilya Loshchilov and Frank Hutter. Sgdr: Stochastic gradient descent with warm restarts. *arXiv preprint arXiv:1608.03983*, 2016.
- Ilya Loshchilov and Frank Hutter. Decoupled weight decay regularization. *arXiv preprint arXiv:1711.05101*, 2017.
- David Mizrahi, Roman Bachmann, Oguzhan Kar, Teresa Yeo, Mingfei Gao, Afshin Dehghan, and Amir Zamir. 4m: Massively multimodal masked modeling. *Advances in Neural Information Processing Systems*, 36:58363–58408, 2023.
- Alexander Quinn Nichol and Prafulla Dhariwal. Improved denoising diffusion probabilistic models. In *International conference on machine learning*, pages 8162–8171. PMLR, 2021.
- Maxime Oquab et al. Dinov2: Learning robust visual features without supervision. *arXiv:2304.07193*, 2023. <https://arxiv.org/abs/2304.07193>.
- Alec Radford, Jong Wook Kim, Chris Hallacy, Aditya Ramesh, Gabriel Goh, Sandhini Agarwal, Girish Sastry, Amanda Askell, Pamela Mishkin, Jack Clark, Gretchen Krueger, and Ilya Sutskever. Learning transferable visual models from natural language supervision. In *Proceedings of the 38th International Conference on Machine Learning (ICML)*, volume 139 of *PMLR*, pages 8748–8763, 2021. <https://proceedings.mlr.press/v139/radford21a/radford21a.pdf>.
- Colin Raffel, Noam Shazeer, Adam Roberts, Katherine Lee, Sharan Narang, Michael Matena, Yanqi Zhou, Wei Li, and Peter J Liu. Exploring the limits of transfer learning with a unified text-to-text transformer. *Journal of machine learning research*, 21(140): 1–67, 2020.
- Aditya Ramesh, Prafulla Dhariwal, Alex Nichol, Casey Chu, and Mark Chen. Hierarchical text-conditional image generation with clip latents. *arXiv preprint arXiv:2204.06125*, 1(2):3, 2022.

- Benjamin Recht, Rebecca Roelofs, Ludwig Schmidt, and Vaishaal Shankar. Do imagenet classifiers generalize to imagenet? In *International conference on machine learning*, pages 5389–5400. PMLR, 2019.
- Robin Rombach, Andreas Blattmann, Dominik Lorenz, Patrick Esser, and Björn Ommer. High-resolution image synthesis with latent diffusion models. In *Proceedings of the IEEE/CVF conference on computer vision and pattern recognition*, pages 10684–10695, 2022.
- Chitwan Saharia, William Chan, Saurabh Saxena, Lala Li, Jay Whang, Emily L Denton, Kamyar Ghasemipour, Raphael Gontijo Lopes, Burcu Karagol Ayan, Tim Salimans, et al. Photorealistic text-to-image diffusion models with deep language understanding. *Advances in neural information processing systems*, 35:36479–36494, 2022.
- Nathan Silberman, Derek Hoiem, Pushmeet Kohli, and Rob Fergus. Indoor segmentation and support inference from rgbd images. In *European conference on computer vision*, pages 746–760. Springer, 2012.
- Oriane Siméoni, Huy V Vo, Maximilian Seitzer, Federico Baldassarre, Maxime Oquab, Cijo Jose, Vasil Khalidov, Marc Szafraniec, Seungeun Yi, Michaël Ramamonjisoa, et al. Dinov3. *arXiv preprint arXiv:2508.10104*, 2025.
- Christian Szegedy, Vincent Vanhoucke, Sergey Ioffe, Jon Shlens, and Zbigniew Wojna. Rethinking the inception architecture for computer vision. In *Proceedings of the IEEE conference on computer vision and pattern recognition*, pages 2818–2826, 2016.
- Mohammad Reza Taesiri, Giang Nguyen, Sarra Habchi, Cor-Paul Bezemer, and Anh Nguyen. Imagenet-hard: The hardest images remaining from a study of the power of zoom and spatial biases in image classification. *Advances in Neural Information Processing Systems*, 36:35878–35953, 2023.
- Ming Tao, Bing-Kun Bao, Hao Tang, and Changsheng Xu. Galip: Generative adversarial clips for text-to-image synthesis. In *Proceedings of the IEEE/CVF conference on computer vision and pattern recognition*, pages 14214–14223, 2023.
- Yonglong Tian, Yue Wang, Dilip Krishnan, Joshua B Tenenbaum, and Phillip Isola. Rethinking few-shot image classification: a good embedding is all you need? In *European conference on computer vision*, pages 266–282. Springer, 2020.
- Yonglong Tian, Lijie Fan, Phillip Isola, Huiwen Chang, and Dilip Krishnan. Stablerep: Synthetic images from text-to-image models make strong visual representation learners. *Advances in Neural Information Processing Systems*, 36:48382–48402, 2023.
- Haohan Wang, Songwei Ge, Zachary Lipton, and Eric P Xing. Learning robust global representations by penalizing local predictive power. In *Advances in Neural Information Processing Systems*, pages 10506–10518, 2019a.
- Yan Wang, Wei-Lun Chao, Kilian Q Weinberger, and Laurens Van Der Maaten. Simpleshot: Revisiting nearest-neighbor classification for few-shot learning. *arXiv preprint arXiv:1911.04623*, 2019b.
- Chengyue Wu, Xiaokang Chen, Zhiyu Wu, Yiyang Ma, Xingchao Liu, Zizheng Pan, Wen Liu, Zhenda Xie, Xingkai Yu, Chong Ruan, et al. Janus: Decoupling visual encoding for unified multimodal understanding and generation. In *Proceedings of the Computer Vision and Pattern Recognition Conference*, pages 12966–12977, 2025a.
- Size Wu, Wenwei Zhang, Lumin Xu, Sheng Jin, Zhonghua Wu, Qingyi Tao, Wentao Liu, Wei Li, and Chen Change Loy. Harmonizing visual representations for unified multimodal understanding and generation. *arXiv preprint arXiv:2503.21979*, 2025b.
- Jinheng Xie, Weijia Mao, Zechen Bai, David Junhao Zhang, Weihao Wang, Kevin Qinghong Lin, Yuchao Gu, Zhijie Chen, Zhenheng Yang, and Mike Zheng Shou. Show-o: One single transformer to unify multimodal understanding and generation. *arXiv preprint arXiv:2408.12528*, 2024.
- Yang You, Igor Gitman, and Boris Ginsburg. Large batch training of convolutional networks. *arXiv preprint arXiv:1708.03888*, 2017.
- Sihyun Yu et al. Representation alignment for generation: Training diffusion transformers is easier than you think. In *ICLR*, 2025. <https://openreview.net/forum?id=DJSZGGZYVi>.
- Sangdoon Yun, Dongyoon Han, Seong Joon Oh, Sanghyuk Chun, Junsuk Choe, and Youngjoon Yoo. Cutmix: Regularization strategy to train strong classifiers with localizable features. In *Proceedings of the IEEE/CVF international conference on computer vision*, pages 6023–6032, 2019.
- Hongyi Zhang, Moustapha Cisse, Yann N Dauphin, and David Lopez-Paz. mixup: Beyond empirical risk minimization. *arXiv preprint arXiv:1710.09412*, 2017.
- Yuhui Zhang, Alyssa Unell, Xiaohan Wang, Dhruva Ghosh, Yuchang Su, Ludwig Schmidt, and Serena Yeung-Levy. Why are visually-grounded language models bad at image classification? *Conference on Neural Information Processing Systems (NeurIPS)*, 2024.
- Boyang Zheng, Nanye Ma, Shengbang Tong, and Saining Xie. Diffusion transformers with representation autoencoders. *arXiv preprint arXiv:2510.11690*, 2025.

Bolei Zhou, Hang Zhao, Xavier Puig, Sanja Fidler, Adela Barriuso, and Antonio Torralba. Scene parsing through ade20k dataset. In *Proceedings of the IEEE conference on computer vision and pattern recognition*, pages 633–641, 2017.

Appendix

A Additional Results

A.1 Qualitative Results

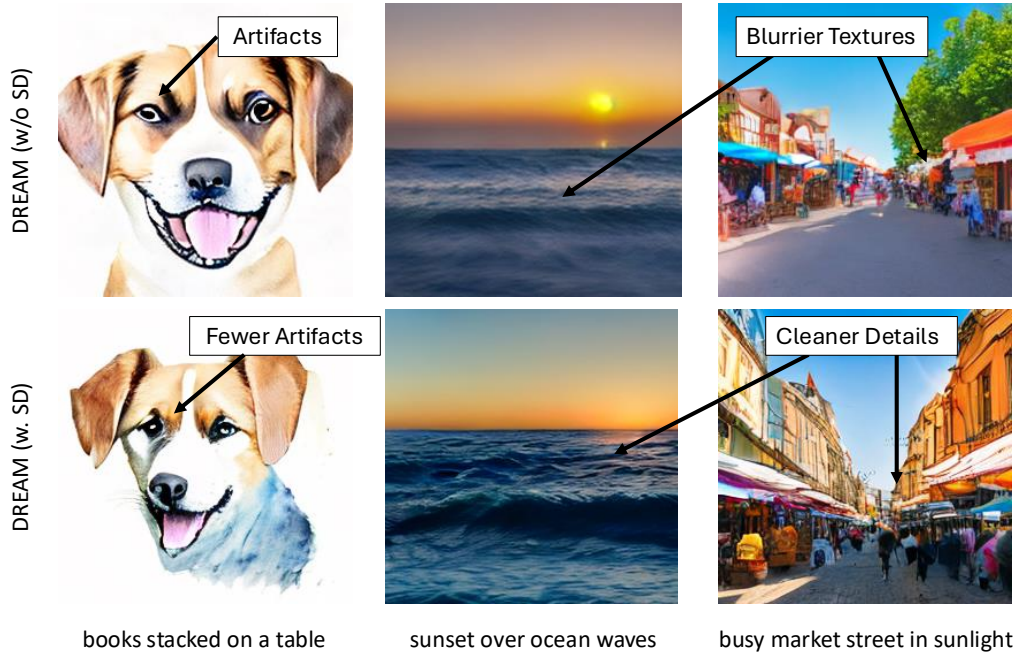


Figure 5 Examples of images generated by DREAM with and without Semantically Aligned Decoding (SD). Without Semantically Aligned Decoding, the outputs exhibit less coherent structure and more low-level blur. Applying Semantically Aligned Decoding produces images with clearer details and improved consistency with the prompt, in line with the gains observed in FID and CLIP scores.

We visualize the generated images to understand the effect of Semantically Aligned Decoding. Fig. 5 shows that with Semantically Aligned Decoding, the generated images tend to exhibit more stable structure and fewer low-level artifacts, consistent with the improvements observed in FID.

This effect aligns with the role of the text-guided retrieval step: since intermediate latents are trained to be semantically aligned with the text encoder, retrieving candidates conditioned on the prompt encourages selecting latents that both match the intended content and reconstruct cleanly. Our semantic segmentation results further indicate that the vision encoder encodes strong object-level cues, suggesting that Semantically Aligned Decoding primarily reinforces this semantic grounding during inference.

As a result, the decoding process naturally favors samples that are semantically coherent with the prompt while maintaining stronger distribution-level realism. Additional qualitative examples are included in Fig. 8, 9, and 10.

A.2 Quantitative Results

A.2.1 Stability of Masking Warm-up

In Fig. 6, we plot Linear Probing accuracy and FID (on CC12M) across training for three masking standard deviations ($\sigma \in 0.35, 0.45, 0.55$). For $\sigma \in 0.45, 0.55$, both metrics improve monotonically throughout training. In contrast, with $\sigma = 0.35$, Linear Probing begins to degrade once masking warm-up ends. This suggests that stable unification requires the masking distribution to exceed a certain variance threshold. A larger standard deviation retains more lightly masked samples after masking warm-up ends, ensuring that enough unmasked visual context is available to compute the CLIP loss and maintain discriminative performance.

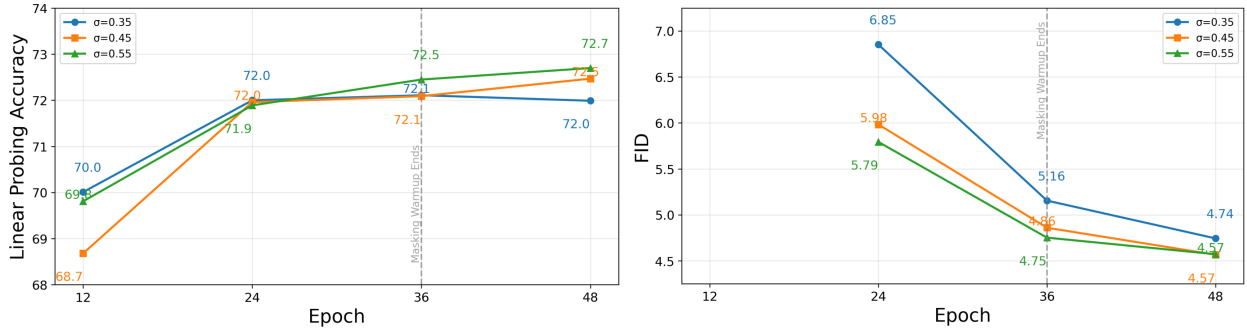


Figure 6 Performance of DREAM across different masking standard deviations. Left: Linear Probing on IN-1K. **Right:** FID on CC12M-50K without Semantically Aligned Decoding. We do not plot the FID values for epoch 12 since training has not converged and FID > 50. The curves show that when $\sigma > 0.35$, both Linear Probing and FID remain stable even after masking warm-up ends.

Overall, these results indicate that given a well-defined masking standard deviation, masking warm-up enables stable joint optimization of discriminative and generative objectives.

A.2.2 Layer to apply REPA loss

Following the method described in Yu et al. (2025), we ablated the layer at which the representations are aligned with a pretrained CLIP ViT-L/16 model, and selected the layer with the lowest FID score. We apply a linear probe on the outputs of the vision encoder. As shown in Table 7, applying REPA at the 6th layer yields the best generative performance, achieving the lowest FID. Interestingly, we observe a consistent trend where deeper alignment layers degrade Linear Probing accuracy.

Table 7 Ablation on the layer to align with pretrained CLIP encoder. Applying the loss on shallower layers yields better linear probing (LP) performance, whereas applying it at deeper layers improves generation quality (lower FID), highlighting the trade-off between representation and generation quality.

	4	6	8
LP \uparrow	58.0	62.5	66.1
FID \downarrow	4.71	4.42	4.76

A.2.3 CLIP vs. DINOv2 Supervision for REPA

Additionally, we compare REPA trained with pretrained CLIP and DINOv2 visual encoders (the default setting in REPA). For fairness, when using DINOv2 supervision, we also ablate and select the optimal feature layer, following the same protocol used for CLIP. We found the optimal layer for REPA loss to be 8th layer.

Table 8 Effect of Visual Backbone

	CLIP	DINOv2
LP \uparrow	62.5	68.4
FID \downarrow	4.42	4.67

As shown in Table 8, REPA supervised with DINOv2 achieves higher linear probing accuracy, indicating stronger semantic representations for downstream recognition tasks. However, this improvement does not translate to better text-to-image generation quality: REPA trained with DINOv2 exhibits worse FID compared to CLIP-supervised REPA. This suggests that while DINOv2 provides stronger category-level representations, CLIP’s text-aligned supervision is more effective for guiding generative models toward high-fidelity, text-consistent image generation.

A.3 Dense Prediction

Table 9 Performance of frozen backbones on dense prediction tasks. Results are reported for semantic segmentation (on ADE20K Zhou et al. (2017)) and depth estimation (on NYU Depth V2 Silberman et al. (2012)) using linear probes Siméoni et al. (2025) mIoU: mean Intersection-over-Union; PixAcc: pixel accuracy; RMSE: root mean squared error; ARel: absolute relative error.

Model	Sem. Seg. (ADE20K)		Depth (NYU Depth V2)	
	mIoU↑	PixAcc↑	RMSE↓	ARel↓
MAR	23.4	70.6	0.75	0.25
FLUID	22.1	69.5	0.76	0.26
CLIP	34.9	75.3	0.64	0.20
REPA	32.7	75.9	0.60	0.19
DREAM	36.8	76.7	0.60	0.19

A.4 Zero-shot Robustness.

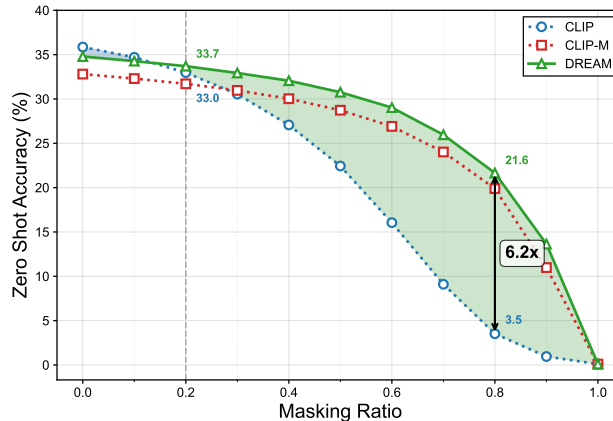


Figure 7 Comparison of zero-shot accuracy for CLIP, CLIP with masking warmup (CLIP-M), and DREAM across varying masking ratios. The green shaded region marks the masking levels at which DREAM surpasses CLIP.

B Additional Ablations

We provide further ablations of hyperparameters that enable the unification of representations. Our ablations show that the performance of the model, both in representation learning and text-to-image generation, remains relatively stable across different values, demonstrating that our masking warm-up framework is stable.

We follow the same default setting as our Analysis Section in the main paper: ablations use DREAM-L trained for 49 epochs on CC12M with the standard configuration: masking standard deviation $\sigma = 0.45$ (which we have established earlier leads to stable joint optimization between representation learning and generation), CLIP loss weight $\lambda = 0.005$, and generation without Semantically Aligned Decoding. We highlight the default settings in gray, and bold the best values in each ablation.

B.1 Masking Schedule

We describe in detail the masking schedules evaluated in Table 4. Unless otherwise noted, all schedules use a truncated Gaussian distribution with a standard deviation of 0.45, a maximum masking ratio of 0.75 for computing the CLIP loss (i.e., 75% of tokens masked), and a minimum masking ratio of 0.5 for computing the MAR loss. The global minimum and maximum masking ratios are fixed at 0 and 1.0, respectively.

- **FX**: Fixed truncated Gaussian distribution centered at 1.0.

- **UNI**: Fixed uniform distribution.
- **CD**: A Gaussian distribution whose mean starts at 1.0 and linearly decreases to 0.0 over the first 36 epochs, after which it remains fixed at 0.0.
- **WM**: A Gaussian distribution whose mean starts at 0.0 and linearly increases to 1.0 over the first 36 epochs, after which it remains fixed at 1.0.

B.2 Standard Deviation of Masking

Table 10 Standard Deviation of Masking Distribution (σ)

	0.35	0.45	0.55	UNI
LP \uparrow	72.0	72.5	72.7	73.1
FID \downarrow	4.74	4.57	4.57	4.88

Our masking warm-up samples masking ratios from $\mathcal{N}(\mu, \sigma^2)$ clipped to $[0, 1]$. To study the effect of variance, we vary σ and additionally include UNI, a schedule that approximates the high-variance limit via a uniform masking distribution.

As shown in Table 10, increasing σ from 0.35 to 0.45–0.55 improves both representation quality and generative performance: Linear Probing increases from 72.0% to 72.7%, while FID decreases from 4.74 to 4.57. Pushing variance to the extreme (UNI) further boosts Linear Probing to 73.1% but degrades FID to 4.88, indicating that overly uniform masking reduces emphasis on the high-masking reconstruction regime needed for strong generation.

Overall, moderate variance in the range $\sigma \in [0.45, 0.55]$ yields the best generative quality while remaining close to the optimal representation performance. Section 4 in the manuscript uses the setting $\sigma = 0.55$, which matches the best FID (4.57) and provides slightly stronger Linear Probing than $\sigma = 0.45$.

Section 4 in the manuscript uses the setting where $\sigma = 0.55$, since it balances between Linear Probing and FID scores.

B.3 Duration of Masking Warm-up

Table 11 Masking Warm-up Duration

	30	36	42
LP \uparrow	72.5	72.5	72.4
FID \downarrow	4.68	4.57	4.71

We ablated the duration of the masking warm-up. As shown in Table 11, Linear Probing accuracy remains largely stable across warm-up durations of 30–42 epochs, showing only minor differences. In contrast, generative quality exhibits a clear optimum: a 36-epoch warm-up achieves the lowest FID (4.57), outperforming both shorter and longer schedules. This suggests that warm-up duration primarily influences generation fidelity rather than discriminative performance, with a moderate length providing the best balance.

B.4 Minimum Ratio for Diffusion Loss

Table 12 Varying Minimum Masking Ratio for Diffusion Loss (γ)

	0	0.25	0.5	0.75
LP \uparrow	72.1	72.7	72.5	71.4
FID \downarrow	4.95	4.73	4.57	7.25

We ablated the minimum masking ratio γ used when computing the diffusion loss. As discussed in Section 3.2, generative training benefits from sufficiently high masking ratios to encourage learning the input distribution. Table 12 shows that

setting $\gamma = 0.5$ (e.g., 50% of the tokens are masked) yields the best generative performance, achieving the lowest FID (4.57) among the tested configurations. In contrast, Linear Probing accuracy decreases as γ increases from 0.25 to 0.75, suggesting that very high minimum masking thresholds reduce the number of low-masking samples seen during training and limit the contribution of reconstruction loss to representation learning. Overall, moderate values of γ provide a better balance between discriminative and generative objectives.

B.5 Maximum Masking Ratio for CLIP Loss

Table 13 Varying Maximum Masking Ratio for CLIP loss (ϕ)

	0.25	0.5	0.75	1.0
LP \uparrow	63.4	70.0	72.5	72.5
FID \downarrow	8.65	4.81	4.57	4.71

We ablated the maximum masking ratio ϕ used when computing the CLIP loss. As shown in Table 13, increasing ϕ from 0.25 to 0.75 leads to consistent gains in Linear Probing accuracy. A larger upper bound allows more samples to retain enough visible content to participate meaningfully in the contrastive objective, strengthening the learned representations.

However, setting $\phi = 1.0$ slightly degrades performance. When images become fully or nearly fully masked, there is insufficient visual context for effective contrastive learning against text, which weakens representation quality.

Overall, the minimum masking ratio for diffusion loss and the maximum masking ratio for CLIP loss together control the degree of overlap between samples that participate in both objectives, thereby influencing the balance between generative reconstruction and discriminative alignment.

B.6 CLIP Loss Weight (λ)

Table 14 Effect of CLIP Loss Weight (λ)

	0.002	0.005	0.01
LP \uparrow	72.1	72.5	72.0
FID \downarrow	4.76	4.57	4.64

Additionally, we also ablated the weight on CLIP loss λ , which balances between representation and generation objectives. Table 14 shows that LP and FID do not change drastically with different weights, demonstrating the stability of DREAM’s framework.

B.7 CLIP Loss on Buffer Tokens

Table 15 Application of CLIP loss.

	All Tokens	Buffer Tokens
LP \uparrow	72.5	72.1
FID \downarrow	4.57	4.57

We further investigate whether restricting the CLIP loss to buffer tokens yields any benefit compared to applying it across both buffer and image tokens. As shown in Table 15, limiting CLIP supervision to buffer tokens slightly reduces Linear Probing accuracy while leaving FID unchanged.

B.8 Layer to apply CLIP loss

Similar to REPA, we also ablated the layer to apply CLIP loss. We apply a linear probe on the final layer of the frozen vision encoder (layer 12). As shown in Table 16, deeper layers monotonically improve Linear Probing (66.6%→72.5%)

Table 16 CLIP loss layer

	6	8	10	12
LP \uparrow	66.6	68.9	70.7	72.5
FID \downarrow	4.51	4.71	4.53	4.57

while FID remains stable (4.51–4.71). The deepest layer (layer 12) achieves both strong discriminative performance and competitive generation quality, indicating that language alignment at the final encoder layer—where the most abstract semantic features reside—successfully produces semantically-grounded representations without interfering with the decoder’s generative capacity.

Notably, our framework demonstrates higher Linear Probing performance than REPA at the same depth (compare with layer 6 in Table 2), since CLIP loss provides stronger text supervision to the visual encoder than REPA.

B.9 Number of Candidates

Table 17 Effect of Number of Candidates (K)

	1	5	9	17
FID \downarrow	4.57	4.51	4.28	4.39
CS \uparrow	29.1	29.8	30.1	30.2

Here, we study the effect of the number of generated candidates on FID and CLIP score under a fixed compute budget of 128 forward encoder (NFE) passes. More candidates mean more partial sequences are spawned earlier in autoregressive decoding, enabling earlier semantic selection.

Table 17 shows that increasing candidates from 1 to 9 improves FID by 6.3% (4.57 \rightarrow 4.28) and CLIP score by 3.4% (29.1 \rightarrow 30.1), with diminishing returns beyond 9. These gains indicate that Semantically Aligned Decoding effectively exploits the encoder’s semantically rich visual representations—accessed via the text encoder—highlighting the synergy between representation learning and generation in DREAM.

C Implementation Details

In the following section, we provide detailed descriptions of our training setup and include pseudocode for DREAM, REPA, and Semantically Aligned Decoding. The full implementation will be made publicly available.

MAR Li et al. (2024) is a class-conditional encoder–decoder model in which the encoder takes class labels as input. FLUID Fan et al. (2024) is a text-to-image model that uses a transformer architecture operating on continuous tokens, which are cross-attended with text tokens.

DREAM draws architectural inspiration from both MAR and FLUID. We adopt the encoder design from MAR but remove the class-conditioning pathway, ensuring that no textual information enters the visual encoder. On the decoder side, we use FLUID’s architecture and introduce text conditioning only at this stage. This prevents shortcuts between visual features and text and ensures that all discriminative and dense-prediction capabilities learned by the encoder originate solely from visual inputs.

We align the encoder’s visual representations with text using the CLIP contrastive loss Radford et al. (2021). Conceptually, DREAM removes text conditioning from the encoder and instead trains the encoder to predict the relevant textual semantics, reintroducing text conditioning only within the decoder.

C.1 Image Tokenizer and Detokenizer

We employ the kl-f8-ft-EMA autoencoder from Stable Diffusion Rombach et al. (2022), a widely used continuous tokenizer. The image is first encoded into a 32×32 latent grid with 4 channels per token. To maintain consistency with the discrete tokenizer, we group each 2×2 block of latent tokens into a single token, resulting in a final sequence of 256 tokens, each with 16 channels. The detokenizer reconstructs the image from the predicted continuous representations.

C.2 ViT Architecture

C.2.1 Vision Encoder

After the tokenizer, the latent sequence length becomes 256. During training, tokens are masked and dropped before being fed into the encoder. We prepend 64 buffer tokens to the unmasked sequence to ensure stability. More specifically, we use standard ViT architecture [Dosovitskiy \(2020\)](#), which consists of a stack of Transformer blocks [Dosovitskiy \(2020\)](#), where each block consists of a multi-head self-attention block and an MLP block. We use two learnable positional embeddings, one added to the input of the encoder and another added to the input of the decoder.

We use features from the encoder output for classification tasks, such as Linear Probing, Few-Shot Transfer Learning, and Fine-tuning. We apply average pooling to the encoder output for linear classification in Linear Probing and Fine-tuning, and we use the corresponding visual embeddings for semantic segmentation and depth estimation.

C.2.2 Text Encoders

We use two text encoders, each serving a distinct role during training. This separation enables direct comparability with prior work and ensures that our contrastive and generative objectives follow established conventions.

For contrastive alignment, captions are tokenized with the OpenAI CLIP tokenizer (77 tokens) and encoded using a CLIP text transformer, following the setup in [Tian et al. \(2023\)](#). The resulting features are projected into the vision encoder’s latent space.

For generation, captions are tokenized with SentencePiece (128 tokens) and encoded using a frozen T5-XXL model [Raffel et al. \(2020\)](#). A lightweight 6-layer text aligner projects the T5 embeddings into the decoder’s latent space, providing conditioning for the decoder. This text-conditioning module follows the design used in FLUID [Fan et al. \(2024\)](#).

C.3 Model Sizes

We evaluate four model scales: **Base (B)**, **Large (L)**, **Huge (H)**, and **Giant (G)**. In all settings, the encoder and decoder share the same number of transformer blocks (e.g., a 32-block model allocates 16 blocks to the encoder and 16 to the decoder).

- **Base (B)**: 24 blocks, hidden size 768
- **Large (L)**: 32 blocks, hidden size 1024
- **Huge (H)**: 40 blocks, hidden size 1280
- **Giant (G)**: 48 blocks, hidden size 1664

The **Huge** configuration corresponds to a ~1B-parameter encoder-decoder model. The **Giant** configuration (~2B parameters in total) provides an encoder with approximately 1B parameters (921M), enabling us to study scaling behavior in the 1B-encoder regime.

C.4 Pre-training

Section [D](#) summarizes the default pre-training configurations used across all experiments. Unless otherwise specified, all models are trained for 49 epochs.

C.4.1 DREAM training

DREAM uses a progressive masking warm-up in which the masking ratio follows a shifting truncated Gaussian distribution. The minimum and maximum masking ratios are fixed at 0 and 1.0, respectively. The mean of the distribution increases linearly from 0 to 1.0 over the first 36 epochs and is then fixed at 1.0 for the remaining epochs. This schedule enables a smooth transition from fully visible inputs to the high-masking regime required for strong generative performance.

C.4.2 REPA training

REPA [Yu et al. \(2025\)](#) was originally proposed for diffusion transformers, where noisy intermediate encoder states are aligned with clean-image features from a pretrained vision encoder. In our adaptation for masked image modeling, we instead align the unmasked tokens of the vision encoder with the corresponding features computed from the full image using a pretrained CLIP-L encoder. This provides REPA-style feature supervision in a manner that is compatible with our masked-token training setup.

C.4.3 CLIP training

Our CLIP baseline is trained without masking for the full 49 epochs.

C.4.4 FLUID and MAR training.

FLUID and MAR baselines are trained for 49 epochs following the MAR masking schedule [Li et al. \(2024\)](#): masking ratios are sampled from a truncated Gaussian centered at 1.0 (100% masking) with a standard deviation of 0.25, bounded to the range [0.7, 1.0]. This setup allows us to directly evaluate the vision encoder and assess the effect of applying text conditioning only in the decoder.

C.5 Inference

C.5.1 Generation

DREAM adopts the MAR [Li et al. \(2024\)](#) decoding procedure, which generates images by predicting a randomly selected set of latent tokens at each step. At inference time, we begin from a fully masked latent sequence and iteratively reduce the masking ratio following a cosine schedule. By default, we use 64 steps in this schedule. In each iteration, DREAM first predicts continuous latent values for all currently masked positions. It then applies token-wise temperature sampling by adding temperature-scaled noise to the predicted latent vectors. Finally, instead of using confidence-based or location-based ordering as in MAGE, DREAM follows MAR’s fully randomized ordering: a subset of positions is sampled uniformly and re-masked to match the target masking ratio for the next iteration. This process progressively refines the latent representation until all positions are filled.

C.5.2 Classifier-free guidance (CFG)

We adopt classifier-free guidance by randomly removing the text condition for 10% of training samples, replacing the prompt with a null token. This trains the model to produce both conditional and unconditional predictions using the same diffusion head.

During inference, we run the model twice: once with the null prompt and once with the given text. This produces the unconditional and conditional representations z_u and z_c . The guided noise prediction is computed as

$$\varepsilon = \varepsilon_{\theta}(x_t | t, z_u) + \omega \cdot (\varepsilon_{\theta}(x_t | t, z_c) - \varepsilon_{\theta}(x_t | t, z_u)),$$

where ω denotes the guidance strength. Since we use a fixed sampling temperature of 1, no additional temperature scaling is applied.

For sampling, we sweep over two CFG schedules: a constant scale and a linearly increasing scale, and report the best CLIP and FID scores.

C.5.3 Semantic Segmentation

For semantic segmentation, we follow the DINOv3 [Siméoni et al. \(2025\)](#) setup. A linear layer is trained on top of the frozen patch features from the vision encoder and evaluated on ADE20K [Zhou et al. \(2017\)](#) (150 categories). We report mean IoU and Pixel Accuracy. The linear head is trained for 40k iterations with a learning rate of 1×10^{-4} using a cosine decay schedule with 1.5k warm-up steps.

C.5.4 Depth Estimation

For depth estimation, we follow the DINOv2 [Oquab et al. \(2023\)](#) protocol. A linear head is trained over frozen patch features and evaluated on NYU Depth v2 [Silberman et al. \(2012\)](#). We report RMSE and ARel. Training uses 38.4k iterations with a learning rate of 3×10^{-4} , a cosine scheduler, and 12.8k warm-up steps.

D Training Settings

Table 18 Pre-training settings for CLIP.

Config	Value
Optimizer	AdamW
Base learning rate	1×10^{-4}
Weight decay	0.02
Momentum	(0.9, 0.95)
Batch size	2048
LR schedule	Constant
Warmup epochs	12
Training epochs	49
Gradient clip	3.0
Label dropout	0.1
Augmentation	Random Horizontal Flipping

Table 19 Pre-training settings for MAR, and FLUID.

Config	Value
Optimizer	AdamW
Base learning rate	1×10^{-4}
Weight decay	0.02
Momentum	(0.9, 0.95)
Batch size	2048
LR schedule	Constant
Warmup epochs	12
Training epochs	49
Gradient clip	3.0
Label dropout	0.1
Augmentation	Random Horizontal Flipping
Masking ratio (min)	0.7
Masking ratio (max)	1.0
Masking ratio (std)	0.25

Table 20 Pre-training settings for REPA.

Config	Value
Optimizer	AdamW
Base learning rate	1×10^{-4}
Weight decay	0.02
Momentum	(0.9, 0.95)
Batch size	2048
LR schedule	Constant
Warmup epochs	12
Training epochs	49
Gradient clip	3.0
Label dropout	0.1
Augmentation	Random Horizontal Flipping
Teacher encoder	CLIP-L
Masking ratio (min)	0.7
Masking ratio (max)	1.0
Masking ratio (std)	0.25
Weight on REPA loss	0.5

Table 21 Pre-training settings for DREAM.

Config	Value
Optimizer	AdamW
Base learning rate	1×10^{-4}
Weight decay	0.04
Momentum	(0.9, 0.95)
Batch size	2048
LR schedule	Constant
Warmup epochs	12
Training epochs	49
Gradient clip	3.0
Label dropout	0.1
Augmentation	Random Horizontal Flipping
Masking ratio (min)	0.0
Masking ratio (max)	1.0
Masking ratio (std)	0.55
Masking warmup epochs	36
Maximum masking for CLIP loss	75%
Minimum masking for diffusion loss	50%
Weight on CLIP loss	0.005

Table 22 Linear Probing Settings.

Config	Value
Optimizer	LARS You et al. (2017)
Base learning rate	0.1 (B), 0.05 (L, H), 0.02 (G)
Weight decay	0
Optimizer momentum	0.9
Batch size	4096
Learning rate schedule	Cosine decay Loshchilov and Hutter (2016)
Warmup epochs	10
Training epochs	90
Augmentation	RandomResizedCrop

Table 23 Fine-tuning Settings.

Config	Value
Optimizer	AdamW Loshchilov and Hutter (2017)
Base learning rate	2.5×10^{-4}
Weight decay	0.05
Optimizer momentum	$\beta_1, \beta_2 = 0.9, 0.999$
Layer-wise LR decay Bao et al. (2021)	0.75
Batch size	1024
Learning rate schedule	Cosine decay Loshchilov and Hutter (2016)
Warmup epochs	5
Training epochs	50
Label smoothing Szegedy et al. (2016)	0.1
Augmentation	RandAug (9, 0.5) Cubuk et al. (2020)
Mixup Zhang et al. (2017)	0.8
CutMix Yun et al. (2019)	1.0
Random erase	0
Drop path Huang et al. (2016)	0.2

Algorithm 1 Training Loop for DREAM

Require: model \mathcal{M} , VAE, CLIP-style text encoder $\mathcal{E}_{\text{clip}}$, conditioning text encoder $\mathcal{E}_{\text{cond}}$, data loader \mathcal{D} , coefficient λ_{clip} , epoch index e

```
1: for each batch  $(\mathbf{I}, \mathbf{T})$  in  $\mathcal{D}$  do
2:    $\mathbf{Z} \leftarrow \text{VAE.Encode}(\mathbf{I})$ 
3:    $\mathbf{t}_{\text{clip}} \leftarrow \mathcal{E}_{\text{clip}}.\text{Encode}(\mathbf{T})$  ▷ text embeddings for CLIP loss
4:    $\mathbf{t}_{\text{cond}} \leftarrow \mathcal{E}_{\text{cond}}.\text{Encode}(\mathbf{T})$  ▷ text embeddings for conditioning
5:    $\mathbf{m} \leftarrow \text{MASKINGSCHEDULER}(\mathbf{Z}, \hat{s} = e + \frac{i}{|\mathcal{D}|})$  ▷ mask depends on  $\mathbf{Z}$  and training step
6:    $\mathbf{Z}_{\text{unmask}} \leftarrow \text{UNMASK}(\mathbf{Z}, \mathbf{m})$  ▷ retain only unmasked tokens

7:    $(\mathbf{H}, \mathbf{R}) \leftarrow \text{ENCODERFORWARD}(\mathbf{Z}_{\text{unmask}})$  ▷ (1) forward encoder on unmasked tokens
8:    $\mathbf{z} \leftarrow \text{DECODERFORWARD}(\mathbf{H}, \mathbf{m}, \mathbf{t}_{\text{cond}})$  ▷ (2) forward decoder conditioned on text

9:    $\mathcal{L}_{\text{mar}} \leftarrow \text{DIFFUSIONLOSS}(\mathbf{z}, \mathbf{Z}, \mathbf{m})$  ▷ (3) MAR / diffusion loss
10:   $\mathbf{f}_{\text{img}} \leftarrow \text{MEANPOOL}(\mathbf{R})$  ▷ mean-pooled encoder image embedding
11:   $\mathcal{L}_{\text{clip}} \leftarrow \text{CLIPLOSS}(\mathbf{f}_{\text{img}}, \mathbf{t}_{\text{clip}})$  ▷ (4) image–text CLIP loss

12:   $\mathcal{L} \leftarrow \mathcal{L}_{\text{mar}} + \lambda_{\text{clip}} \cdot \mathcal{L}_{\text{clip}}$  ▷ (5) combined objective
13:   $\mathcal{L}.\text{BACKPROP}()$  ▷ (6) backpropagation step
14: end for
```

Algorithm 2 Training Loop for REPA Baseline, Implemented for Masked Image Modeling

Require: model \mathcal{M} , VAE, conditioning text encoder $\mathcal{E}_{\text{cond}}$, REPA teacher encoder $\mathcal{E}_{\text{teacher}}$, data loader \mathcal{D} , coefficient λ_{repa} , epoch index e

```
1: for each batch  $(\mathbf{I}, \mathbf{T})$  in  $\mathcal{D}$  do
2:    $\mathbf{Z} \leftarrow \text{VAE.Encode}(\mathbf{I})$ 
3:    $\mathbf{t}_{\text{cond}} \leftarrow \mathcal{E}_{\text{cond}}.\text{Encode}(\mathbf{T})$  ▷ text embedding used solely for decoder conditioning
4:    $\mathbf{m} \leftarrow \text{MASKINGSCHEDULER}(\mathbf{Z}, \hat{s} = e + \frac{i}{|\mathcal{D}|})$  ▷ mask depends on  $\mathbf{Z}$  and training step
5:    $\mathbf{Z}_{\text{unmask}} \leftarrow \text{UNMASK}(\mathbf{Z}, \mathbf{m})$  ▷ retain only unmasked tokens

6:    $(\mathbf{H}, \mathbf{R}) \leftarrow \text{ENCODERFORWARD}(\mathbf{Z}_{\text{unmask}})$  ▷ (1) encoder forward on unmasked tokens
7:    $\mathbf{z} \leftarrow \text{DECODERFORWARD}(\mathbf{H}, \mathbf{m}, \mathbf{t}_{\text{cond}})$  ▷ (2) decoder reconstructs masked tokens

8:    $\mathcal{L}_{\text{mar}} \leftarrow \text{DIFFUSIONLOSS}(\mathbf{z}, \mathbf{Z}, \mathbf{m})$  ▷ (3) MAR / diffusion reconstruction loss

9:    $\mathbf{R}_{\text{teacher}} \leftarrow \mathcal{E}_{\text{teacher}}.\text{FORWARDFEATURES}(\mathbf{I})$  ▷ teacher encoder features
10:   $\mathcal{L}_{\text{repa}} \leftarrow \text{REPALOSS}(\mathbf{R}, \mathbf{R}_{\text{teacher}})$  ▷ (4) REPA encoder alignment loss

11:   $\mathcal{L} \leftarrow \mathcal{L}_{\text{mar}} + \lambda_{\text{repa}} \cdot \mathcal{L}_{\text{repa}}$  ▷ (5) combined MAR + REPA objective
12:   $\mathcal{L}.\text{BACKPROP}()$  ▷ (6) backpropagation step
13: end for
```

Algorithm 3 Semantically Aligned Decoding

Require: Number of candidates N , threshold step T , total steps S , text \mathcal{Y}

```
1: Initialize candidate states  $\{(\mathbf{x}^{(n)}, \mathbf{m}^{(n)})\}_{n=1}^N$ 
2: for step = 0 to  $S-1$  do
3:   if step <  $T$  then                                     ▶ 1) Generate  $N$  candidates up to step  $T$ 
4:     for  $n = 1$  to  $N$  do
5:        $(\mathbf{x}^{(n)}, \mathbf{m}^{(n)}) \leftarrow \text{DecodeStep}(\mathbf{x}^{(n)}, \mathbf{m}^{(n)}, \mathcal{Y})$ 
6:     end for
7:   else if step =  $T$  then                                   ▶ 2) Score with text and retrieve best
8:     for  $n = 1$  to  $N$  do
9:        $s_n \leftarrow \text{CLIPScore}(\mathbf{x}^{(n)}, \mathcal{Y})$ 
10:    end for
11:     $n^* \leftarrow \arg \max_n s_n$ 
12:     $(\mathbf{x}, \mathbf{m}) \leftarrow (\mathbf{x}^{(n^*)}, \mathbf{m}^{(n^*)})$ 
13:  else                                                       ▶ 3) Continue decoding best candidate
14:     $(\mathbf{x}, \mathbf{m}) \leftarrow \text{DecodeStep}(\mathbf{x}, \mathbf{m}, \mathcal{Y})$ 
15:  end if
16: end for
17: return Unpatchify( $\mathbf{x}$ )
```



Hiking along the Chipola River



Skinny Broccoli and Mixed Vegetable Stir Fry - Skip takeout and make your own fast, easy, and healthy stir fry! Think of all the money and calories you'll save!!



Home is Where the Art is IX <PERSON>



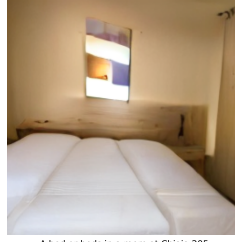
View of rooftop of Church of the Holy Sepulchre in Old City, Old City, UNESCO World Heritage Site, Jerusalem, Israel, Middle East



Shared Zone - road walking through some of Innes National Park



A soup bowl served with Egg drop soup topped with scallions and fried noodle



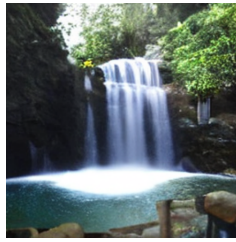
A bed or beds in a room at Chiaia 205



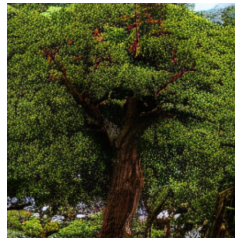
Unusual lighting can make the atmosphere in the bathroom too



The Ghost (bike) Rider Comic Book Characters, Comic Books, Ghost Rider 2, Scary, Creepy, Cycling Art, Road Cycling, Bicycle Art, Bike Rider



The Hunas Falls Hotel: Starting point of the waterfall



Tree Photograph - The Manzanita Tree by <PERSON>



HD Wallpaper American Flag with high-resolution 1920x1080 pixel. You can use this wallpaper 1920x1080



This Snow Covered Abandoned Mall Has Been Forgotten By Time



Wallpapers Anime, My Hero Academia, Blood, All Might Desktop Picture



The Art Print featuring the painting The Garden at Bougival by <PERSON>



The Porcelain Jars - Vigan, Ilocos Sur



The Famous church of the good shepherd photographed in the night with Milky way in the background



Fruit Still Life With Two Peaches And Blue And Green Grapes On The Branch And A Vine Leaf Artwork by <PERSON>



The Wizard Nebula: Sharpless 142



Local visual arts fans have a treat awaiting them at the Asheville Mall through April 28.

Figure 8 Images generated by DREAM-L (0.57B) model from CC12M captions with CFG = 5.0.



Hiking along the Chipola River



Skinny Broccoli and Mixed Vegetable Stir Fry - Skip takeout and make your own fast, easy, and healthy stir fry! Think of all the money and calories you'll save!!



Home is Where the Art is IX <PERSON>



View of rooftop of Church of the Holy Sepulchre in Old City, Old City, UNESCO World Heritage Site, Jerusalem, Israel, Middle East



Shared Zone - road walking through some of Innes National Park



A soup bowl served with Egg drop soup topped with scallions and fried noodle



A bed or beds in a room at Chiaia 205



Unusual lighting can make the atmosphere in the bathroom too



The Ghost (bike) Rider Comic Book Characters, Comic Books, Ghost Rider 2, Scary, Creepy, Cycling Art, Road Cycling, Bicycle Art, bike Rider



The Hunas Falls Hotel: Starting point of the waterfall



Tree Photograph - The Manzanita Tree by <PERSON>



HD Wallpaper American Flag with high-resolution 1920x1080 pixel. You can use this wallpaper 1920x1080



This Snow Covered Abandoned Mall Has Been Forgotten By Time



Wallpapers Anime, My Hero Academia, Blood, All Might Desktop Picture



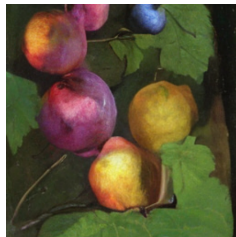
The Art Print featuring the painting The Garden at Bougival by <PERSON>



The Porcelain Jars - Vigan, Ilocos Sur



The Famous church of the good shepherd photographed in the night with Milky way in the background



Fruit Still Life With Two Peaches And Blue And Green Grapes On The Branch And A Vine Leaf Artwork by <PERSON>



The Wizard Nebula: Sharpless 142



Local visual arts fans have a treat awaiting them at the Asheville Mall through April 28.

Figure 9 Images generated by DREAM-H (1.1B) model from CC12M captions with CFG = 5.0.



Hiking along the Chipola River



Skinny Broccoli and Mixed Vegetable Stir Fry - Skip takeout and make your own fast, easy, and healthy stir fry! Think of all the money and calories you'll save!!



Home is Where the Art is IX <PERSON>



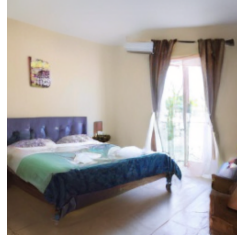
View of rooftop of Church of the Holy Sepulchre in Old City, Old City, UNESCO World Heritage Site, Jerusalem, Israel, Middle East



Shared Zone - road walking through some of Innes National Park



A soup bowl served with Egg drop soup topped with scallions and fried noodle



A bed or beds in a room at Chiaia 205



Unusual lighting can make the atmosphere in the bathroom too



The Ghost (bike) Rider Comic Book Characters, Comic Books, Ghost Rider 2, Scary, Creepy, Cycling Art, Road Cycling, Bicycle Art, Bike Rider



The Hunas Falls Hotel: Starting point of the waterfall



Tree Photograph - The Manzanita Tree by <PERSON>



HD Wallpaper American Flag with high-resolution 1920x1080 pixel. You can use this wallpaper 1920x1080



This Snow Covered Abandoned Mall Has Been Forgotten By Time



Wallpapers Anime, My Hero Academia, Blood, All Might Desktop Picture



The Art Print featuring the painting The Garden at Bougival by <PERSON>



The Porcelain Jars - Vigan, Ilocos Sur



The Famous church of the good shepherd photographed in the night with Milky way in the background



Fruit Still Life With Two Peaches And Blue And Green Grapes On The Branch And A Vine Leaf Artwork by <PERSON>



The Wizard Nebula: Sharpless 142



Local visual arts fans have a treat awaiting them at the Asheville Mall through April 28.

Figure 10 Images generated by DREAM-G (2.4B) model from CC12M captions with CFG = 5.0.